Coupled Systems Mechanics, *Vol. 14, No. 4 (2025) 395-412*
https://doi.org/10.12989/csm.2025.14.4.395

Taking into account the inertia terms in lengthwise fracture analysis of moving bars

Victor I. Rizov*

Department of Technical Mechanics, University of Architecture, Civil Engineering and Geodesy, 1 Chr. Smirnensky Blvd., 1046-Sofia, Bulgaria

(Received November 14, 2024, Revised September 4, 2025, Accepted September 5, 2025)

Abstract. As known, when structural members and components perform motion with acceleration they are subjected to influence of inertia terms. These terms play an important role when assessing different aspects of the behavior of engineering structures. This paper treats the problem of the lengthwise fracture behavior of continuously inhomogeneous bars which move in horizontal direction and at the same time rotate around a longitudinal axis. Particular attention is paid to the problem of determining the inertia terms that act upon the bars. Since the bars under consideration are continuously inhomogeneous in both longitudinal and transversal directions, the mass per unit area change continuously along the length and thickness of the bars. The inertia terms also change continuously in the length and thickness directions. The bars have non-linear elastic behavior. The parameters of the non-linear constitutive law used in this paper change continuously along the bars length and thickness. The integral *J* is applied for analyzing the lengthwise fracture in the bars under the forces of inertia. The strain energy release rate (SERR) is derived for verification of the integral *J*. The effects of the parameters of the laws for motion of the bars on the lengthwise fracture are evaluated and reported in form of diagrams presenting the change of the integral *J*. Assessments of the influence of the change of the mass per unit area and the parameters of the constitutive law along the length and thickness of the bars on the lengthwise fracture are made too.

Keywords: acceleration; inertia terms; law of motion; lengthwise crack; material inhomogeneity; moving bar

1. Introduction

Significant advances in developing of new structural materials that have been achieved by engineering community around the globe in the recent decades are very important for expanding our technological capabilities and improving the quality of life. It is worth nothing that the quick progress in various areas of modern engineering depends on creating of novel and efficient composite materials with desirable properties. In this respect, continuously inhomogeneous materials like the functionally graded ones thanks to their unique and superior properties take a very important place in the group of up-to-date composites materials (Tutuncu 2007, Yildirim and

*Corresponding author, Professor, E-mail: v_rizov_fhe@uacg.bg

http://www.techno-press.org/?journal=csm&subpage=8 ISSN: 2234-2184 (Print), 2234-2192 (Online)

Tutuncu 2019). For instance, these materials have high performance capacities since their properties change smoothly in a desired way which is one of their most important advantages over traditional engineering materials like metals or fibre reinforced composites. Currently, the use of continuously inhomogeneous materials for manufacturing of various structural members and mechanical components is increasing rapidly worldwide (Celebi and Tutuncu 2011, Djillali Mokhefi *et al.* 2024, Gasik 2010, Hedia *et al.* 2014, Hirai and Chen 1999, Mahamood and Akinlabi 2017, Markworth *et al.* 1995, Miyamoto *et al.* 1999, Nemat-Allal *et al.* 2011, Rezaiee-Pajand *et al.* 2018, Rezaiee-Pajand *et al.* 2018). This fact accelerates the research in the field of mechanics and technology of these novel composites (Mokhtar Ellali *et al.* 2024, Rezaiee-Pajand and Masoodi 2019, Tutuncu and Ozturk 2001, Tutuncu and Temel 2013). The substantial advance made in the area of theory, modeling, analysis, design, application and processing of functionally graded materials and structures is clearly indicated by the high number of scientific publications on this subject (Benferhat Rabia *et al.* 2023, Cetin *et al.* 2024, Hung *et al.* 2023, Hung *et al.* 2024, Phung-Van *et al.* 2023, Phung-Van *et al.* 2024, Rezaiee-Pajand *et al.* 2022, Rizov 2017, Rizov and Altenbach 2019, Rizov 2022). Although the diverse investigations that have been performed in the recent decades contribute significantly for ongoing progress in the science and technology of continuously inhomogeneous materials, there are many unsolved problems in this area. In particular, a variety of issues related to the strength and fracture of structural members and components made by continuously inhomogeneous materials with non-linear elastic behavior have not been studied sufficiently.

For example, observations of the failure behavior of various inhomogeneous structural members and components including the moving ones in many cases reveal existence of lengthwise cracks, i.e., cracks located in longitudinal direction. The origin of the lengthwise fracture phenomena lies in the technologies used for manufacturing of continuously inhomogeneous (functionally graded) materials and structural members. One of these technologies in essence represents building-up the structural members layer-by-layer (Mahamood and Akinlabi 2017). Namely this generates conditions for appearance of lengthwise cracks. Lengthwise fracture phenomena certainly depend on many factors like structural member geometry, material parameters (in particular, for continuously inhomogeneous materials, the distribution of the material properties in a structural member play an important role), character of the external loading, boundary conditions, material non-linearity, etc. (Dolgov 2005, 2016, 2024, Dowling 2013, Rizov 2021, 2024, 2025). The lengthwise cracks induce a significant weakness of the structural members and components. As a result of this, the load carrying capacity of the structures reduces considerably. Besides, very often the structural collapse is triggered by lengthwise cracks. Assessing the safety of a continuously inhomogeneous structural system necessitates development of analyses of its lengthwise fracture behavior which take into account a variety of factors and parameters. Many structural members and components perform motion with acceleration that induces inertia terms which affect different aspects of the behavior of structures including lengthwise fracture. Therefore, there exists a demand for approaches for analysis of lengthwise fracture in continuously inhomogeneous structures which are acted upon by forces of inertia.

In this paper, our attention is focused on the lengthwise fracture problem in continuously inhomogeneous moving bars. In particular, we consider bars that move in horizontal direction simultaneously with rotation around a longitudinal axis. The bars are continuously inhomogeneous in both length and thickness. The mechanical behavior of the bars material is treated by using a non-linear stress-strain constitutive law. The mass per unit area and the parameters of the constitutive law change continuously along the length and thickness of the bars due to the material

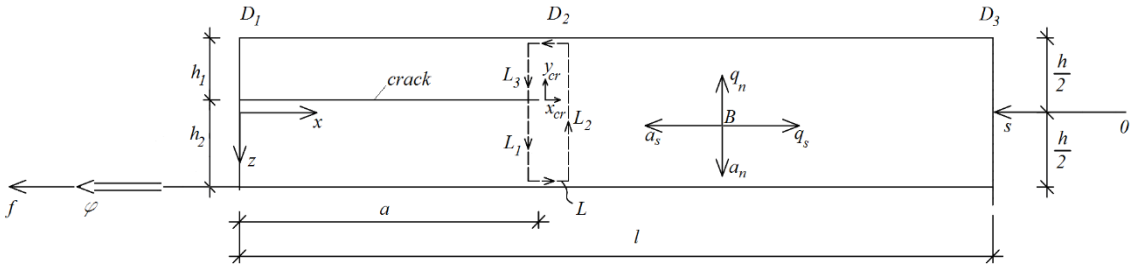

Fig. 1 Moving bar with a lengthwise crack

inhomogeneity. The length to thickness ratio of the bars treated here is high. Special attention is paid to determination of inertia terms. As known, these terms are functions of the mass and acceleration. In the case under consideration the inertia terms change continuously along the bar length and thickness since both the mass per unit area and the acceleration are continuous functions of the two coordinates, x and z. The lengthwise fracture in the bars under the inertia terms is analyzed by the integral J. The analysis is confirmed by deriving the SERR. The influence of the parameters of the laws for motion of the bar, the change of the mass per unit area and the parameters of the constitutive law along the length and thickness of the bars on the lengthwise fracture is assessed. The results are presented in forms of diagrams illustrating the change of the value of the integral J.

2. Lengthwise fracture analysis of bars under forces of inertia

Consider the horizontal bar depicted in Fig. 1. The length and thickness of this bar are denoted as l and h, respectively. The bar is rectangular (its cross-section is depicted in Fig. 2). There is a lengthwise crack in portion, D_1D_2, of the bar as depicted in Fig. 1. This bar movies in horizontal direction leftward according to the law, s, defined by formula (1).

$$s = \beta t^{\delta}, \tag{1}$$

where t is time, β and δ are parameters. The axis, s, is depicted in Fig. 1.

Likewise, the bar rotates around the horizontal axis, f, according to the law, ϕ, defined by (2), i.e.

$$\varphi = \lambda t, \tag{2}$$

where ϕ is the angle of rotation, λ is a parameter. The axis, f, and the angle of rotation are depicted in Fig. 1.

The bar is continuously inhomogeneous along its length and thickness. The mass per unit area of the bar is denoted by m. Due to material inhomogeneity, m is a continuous function of the coordinates, x and z, i.e.

$$m = m(x, z). \tag{3}$$

The coordinate axes, x and z, are depicted in Fig. 1. In this paper, the change of m along the length and thickness of the bar obeys the laws defined by formulas (4), (5) and (6).

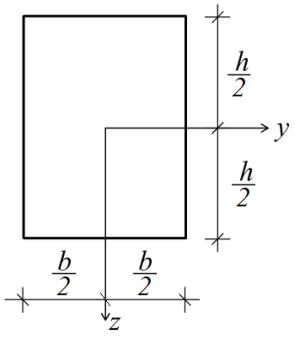

Fig. 2 Cross-section of the bar

$$m = m_{lft} + \frac{m_{rgh} - m_{lft}}{l^{\eta}} x^{\eta}, \tag{4}$$

$$m_{lft} = m_{lup} + \frac{m_{llw} - m_{lup}}{h^{\mu}} \left(\frac{h}{2} + z \right)^{\mu}, \tag{5}$$

$$m_{rgh} = m_{rup} + \frac{m_{rlw} - m_{rup}}{h^{\rho}} \left(\frac{h}{2} + z \right)^{\rho}, \tag{6}$$

where

$$0 \le x \le l, \tag{7}$$

$$-\frac{h}{2} \le z \le \frac{h}{2}. \tag{8}$$

In the above formulas, m_{lft} and m_{rgh} are the masses per unit area in the left-hand and right-hand ends of the bar, m_{lup} and m_{llw} are the values of m_{lft} in the upper and lower vertex in the left-hand end of the bar, m_{rup} and m_{rlw} are the values of m_{rgh} in the upper and lower vertex in the right-hand end of the bar, η, μ and ρ are parameters.

In order to derive the inertia terms, we calculate the acceleration in an arbitrary point, B, of the bar with coordinates, x and z. For this purpose, first we treat the motion of the bar in horizontal direction. By differentiating of the law of motion (1) for time, we obtain the following expressions for the velocity, v_s, and acceleration, a_s

$$v_s = \beta\delta t^{\delta-1}, \tag{9}$$

$$a_s = \beta\delta(\delta-1)t^{\delta-2}. \tag{10}$$

Both v_s and a_s are directed leftward. The velocity (9) and the acceleration (10) are the same in each point of the bar.

Next, we treat the rotation of the bar around the axis, f. The first and second derivatives of the law of rotation (2) with respect to time are expressed by formulas (11) and (12), respectively.

$$\omega = \lambda, \tag{11}$$

$$\alpha = 0. \tag{12}$$

Here, ω and α are the angular velocity and angular acceleration of the bar. The normal acceleration, a_n, of an arbitrary point of the bar is found by the next formula.

$$a_n = \omega^2\left(\frac{h}{2} - z\right), \tag{13}$$

where

$$-\frac{h}{2} \le z \le \frac{h}{2}. \tag{14}$$

The normal acceleration (13) is directed downward. The accelerations, a_s and a_n, of an arbitrary point, B, in the bar are depicted in Fig. 1.

The accelerations, a_s and a_n, are used to derive the inertia terms by applying D'Alembert's principle. Hence, the densities of the forces of inertia, q_s and q_n, associated with accelerations, a_s and a_n, are derived by formulas (15) and (16), respectively.

$$q_s = -ma_s, \tag{15}$$

$$q_n = -ma_n. \tag{16}$$

By taking into account expressions (10) and (13), formulas (15) and (16) are transformed as given below.

$$q_s = -m\beta\delta(\delta - 1)t^{\delta-2}, \tag{17}$$

$$q_n = -m\omega^2\left(\frac{h}{2} - z\right). \tag{18}$$

The densities of the forces of inertia, q_s and q_n, in an arbitrary point, B, of the bar are depicted in Fig. 1. It should be specified that q_s and q_n are continuous functions of the coordinates because m is a continuous function of x and z. Besides, a_n is also a continuous function of z.

The elementary forces of inertia, $d\Phi_{qs}$ and $d\Phi_{qn}$, are presented by the following formulas:

$$d\Phi_{qs} = q_s dxdz, \tag{19}$$

$$d\Phi_{qn} = q_n dxdz. \tag{20}$$

Dependences (17) and (18) are inserted in formulas (19) and (20). Thus, the elementary forces of inertia are expressed as given below.

$$d\Phi_{qs} = -m\beta\delta(\delta - 1)t^{\delta-2}dxdz, \tag{21}$$

$$d\Phi_{qn} = -m\omega^2\left(\frac{h}{2} - z\right)dxdz. \tag{22}$$

Form view point of its mechanical behavior, the bar under consideration is non-linear elastic. The non-linear constitutive law used for treating the bar mechanical behavior is presented in formula (23) (Tsankov 1996).

$$\sigma = H\varepsilon^{\gamma} - T\varepsilon^{\phi}, \tag{23}$$

where σ is the stress, ε is the strain, H, γ, T and φ are parameters. Because of the continuous material inhomogeneity of the bar, H, γ, T and φ change smoothly along the length and thickness of the bar. This change is described by the laws presented in the next formulas.

$$H = H_{lft} + \frac{H_{rgh} - H_{lft}}{l^{\psi_H}} x^{\psi_H}, \tag{24}$$

$$H_{lft} = H_{lup} + \frac{H_{llw} - H_{lup}}{h^{\theta_H}} \left(\frac{h}{2} + z \right)^{\theta_H}, \tag{25}$$

$$H_{rgh} = H_{rup} + \frac{H_{rlw} - H_{rup}}{h^{\chi_H}} \left(\frac{h}{2} + z \right)^{\chi_H}, \tag{26}$$

$$\gamma = \gamma_{lft} + \frac{\gamma_{rgh} - \gamma_{lft}}{l^{\psi_\gamma}} x^{\psi_\gamma}, \tag{27}$$

$$\gamma_{lft} = \gamma_{lup} + \frac{\gamma_{llw} - \gamma_{lup}}{h^{\theta_\gamma}} \left(\frac{h}{2} + z \right)^{\theta_\gamma}, \tag{28}$$

$$\gamma_{rgh} = \gamma_{rup} + \frac{\gamma_{rlw} - \gamma_{rup}}{h^{\chi_\gamma}} \left(\frac{h}{2} + z \right)^{\chi_\gamma}, \tag{29}$$

$$T = T_{lft} + \frac{T_{rgh} - T_{lft}}{l^{\psi_T}} x^{\psi_T}, \tag{30}$$

$$T_{lft} = T_{lup} + \frac{T_{llw} - T_{lup}}{h^{\theta_T}} \left(\frac{h}{2} + z \right)^{\theta_T}, \tag{31}$$

$$T_{rgh} = T_{rup} + \frac{T_{rlw} - T_{rup}}{h^{\chi_T}} \left(\frac{h}{2} + z \right)^{\chi_T}, \tag{32}$$

$$\phi = \phi_{lft} + \frac{\phi_{rgh} - \phi_{lft}}{l^{\psi_\phi}} x^{\psi_\phi}, \tag{33}$$

$$\phi_{lft} = \phi_{lup} + \frac{\phi_{llw} - \phi_{lup}}{h^{\theta_\phi}} \left(\frac{h}{2} + z \right)^{\theta_\phi}, \tag{34}$$

$$\phi_{rgh} = \phi_{rup} + \frac{\phi_{rlw} - \phi_{rup}}{h^{\chi_\phi}} \left(\frac{h}{2} + z \right)^{\chi_\phi}, \tag{35}$$

where

$$0 \le x \le l, \tag{36}$$

$$-\frac{h}{2} \le z \le \frac{h}{2}. \tag{37}$$

In formulas (24)-(35), H_{lft} and H_{rgh} are the values of H in the left-hand and right-hand ends of the bar, H_{lup} and H_{llw} are the values of H_{lft} in the upper and lower vertex in left-hand end of the bar, H_{rup} and H_{rlw} are the values of H_{rgh} in the upper and lower vertex in right-hand end of the bar, γ_{lft} and γ_{rgh} are the values of γ in the left-hand and right-hand ends of the bar, γ_{lup} and γ_{llw} are the values of γ_{lft} in the upper and lower vertex in left-hand end of the bar, γ_{rup} and γ_{rlw} are the values of γ_{rgh} in the upper and lower vertex in right-hand end of the bar, T_{lft} and T_{rgh} are the values of T in the left-hand and right-hand ends of the bar, T_{lup} and T_{llw} are the values of T_{lft} in the upper and lower vertex in left-hand end of the bar, T_{rup} and T_{rlw} are the values of T_{rgh} in the upper and lower vertex in right-hand end of the bar, φ_{lft} and φ_{rgh} are the values of φ in the left-hand and right-hand ends of the bar, φ_{lup} and φ_{llw} are the values of φ_{lft} in the upper and lower vertex in left-hand end of the bar, φ_{rup} and φ_{rlw} are the values of φ_{rgh} in the upper and lower vertex in right-hand end of the bar, ψ_H, θ_H, χ_H, ψ_γ, θ_γ, χ_γ, ψ_T, θ_T, χ_T, ψ_φ, θ_φ and χ_φ are parameters.

The aim of this paper is to analyze the lengthwise fracture when the bar is acted upon by the forces of inertia. For this purpose, the integral J is applied (Broek 1986). This integral is solved along the contour of integration, $L_1L_2L_3$. Since the contour has three segments, L_1, L_2 and L_3, as depicted in Fig. 1, the solution of J is derived as given below.

$$J = J_{L1} + J_{L2} + J_{L3}, \tag{38}$$

where J_{L1}, J_{L2} and J_{L3}, are the solutions in the integration contour segments, L_1, L_2 and L_3, respectively.

J_{L1} is written as given in formula (39).

$$J_{L1}=\int\left[u_{0L1}\cos\alpha_{L1}-\left(p_{xcrL1}\frac{\partial u_{L1}}{\partial x_{cr}}+p_{ycrL1}\frac{\partial v_{L1}}{\partial x_{cr}}\right)\right]dL_1 \quad , \tag{39}$$

where u_{0L1} is the specific strain energy calculated by formula (40), i.e.

$$u_{0L1} = \int \sigma d\varepsilon \ . \tag{40}$$

Here, σ is function of ε (refer to (23)).

α_{S1} is the angle between the outward normal vector of the segment, L_1, of the integration contour and axis, x_{cr}. Formula (41) is used for determining of $cos\ \alpha_{S1}$, i.e.

$$\cos\alpha_{S1} = -1. \tag{41}$$

The other components of J_{L1} are derived by the next formulas.

$$p_{xcrL1} = -\sigma \ , \tag{42}$$

$$\frac{\partial u_{L1}}{\partial x_{cr}} = \varepsilon \ , \tag{43}$$

$$p_{ycrL1} = 0, \tag{44}$$

$$dL_1 = dz_1, \tag{45}$$

where u_{L1} is the horizontal component of the displacements of the integration contour, p_{ycrL1} is the vertical component of the stress along the integration contour, dL_1 is an elementary portion of the integration contour, z_1 is the vertical centric axis of the crack lower arm. Apparently

$$-\frac{h_2}{2} \le z_1 \le \frac{h_2}{2}, \tag{46}$$

where h_2 is the thickness of the crack lower arm (Fig. 1).

The quantities, σ and ε, involved in formulas (40), (42) and (43) are analyzed by considering the equilibrium of the crack lower arm under the forces of inertia. For this purpose, Eqs. (47) and (48) are used.

$$N = b\int_{-\frac{h_2}{2}}^{\frac{h_2}{2}} \sigma dz_1, \tag{47}$$

$$M = b\int_{-\frac{h_2}{2}}^{\frac{h_2}{2}} \sigma z_1 dz_1, \tag{48}$$

where N and M are the axial force and the bending moment, b is the bar width. Formulas (49) and (50) are applied for deriving the axial force and the bending moment (these formulas are obtained by considering the equilibrium of the crack lower arm under the forces of inertia).

$$N = b\int_0^a \left(\int_{-\frac{h_2}{2}}^{\frac{h_2}{2}} -m\beta\delta(\delta-1)t^{\delta-2} dz_1 \right) dx, \tag{49}$$

$$M = b\int_0^a \left\{ \int_{-\frac{h_2}{2}}^{\frac{h_2}{2}} \left[-m\beta\delta(\delta-1)t^{\delta-2} z_1 + m\omega^2 \left(\frac{h_2}{2} - z_1 \right)(a-x) \right] dz_1 \right\} dx, \tag{50}$$

where a is the length of the crack.

The strain that is involved in Eqs. (47) and (48) via the constitutive law (23) is treated by the formula given below.

$$\varepsilon = \kappa_1 (z_1 - z_{1n}), \tag{51}$$

where

$$-\frac{h_2}{2} \le z_1 \le \frac{h_2}{2}. \tag{52}$$

Here, κ_1 and z_1 are the curvature and the coordinate of the neutral axis in the cross-section of the crack lower arm, respectively. κ_1 and z_1 are determined from Eqs. (47) and (48) by the MatLab. Then, the integral in formula (39) is solved by the MatLab.

J_{L2} is derived by using formula (53).

$$J_{L2}=\int\left[u_{0L2}\cos\alpha_{L2}-\left(p_{xcrL2}\frac{\partial u_{L2}}{\partial x_{cr}}+p_{ycrL2}\frac{\partial v_{L2}}{\partial x_{cr}}\right)\right]dL_2\ , \tag{53}$$

where

$$u_{0L2}=\int\sigma_{L2}d\varepsilon_{L2}\,, \tag{54}$$

$$\cos\alpha_{L2}=1, \tag{55}$$

$$p_{xcrL2}=\sigma_{L2}\,, \tag{56}$$

$$\frac{\partial u_{L2}}{\partial x_{cr}}=\varepsilon_{L2}\,, \tag{57}$$

$$p_{ycrL2}=0\,, \tag{58}$$

$$dL_2=-dz_2\,. \tag{59}$$

Here, z_2 is the vertical centric axis of the cross-section of the intact portion, D_2D_3, of the bar. It is obvious that

$$-\frac{h}{2}\le z_2\le\frac{h}{2}\,. \tag{60}$$

The quantities, σ_{L2} and ε_{L2}, involved in formulas (54), (56) and (57) are analyzed through Eqs. (61) and (62).

$$N_{L2}=b\int_{-\frac{h}{2}}^{\frac{h}{2}}\sigma_{L2}dz_2\,, \tag{61}$$

$$M_{L2}=b\int_{-\frac{h}{2}}^{\frac{h}{2}}\sigma_{L2}z_2dz_2\,, \tag{62}$$

where σ_{L2} is related to ε_{L2} by replacing of ε with ε_{L2} in law (23). The strain, ε_{L2}, is written as given below.

$$\varepsilon_{L2}=\kappa_2\left(z_2-z_{2n}\right), \tag{63}$$

where κ_2 and z_2 are the curvature and the coordinate of the neutral axis in section, L_2.

The axial force, N_{L2}, and the bending moment, M_{L2}, are determined by considering the

equilibrium of the bar portion, D_1D_2, under the forces of inertia, i.e.

$$N_{L2}=b\int_0^a\left(\int_{-\frac{h}{2}}^{\frac{h}{2}}-m\beta\delta(\delta-1)t^{\delta-2}dz_2\right)dx, \tag{64}$$

$$M_{L2}=b\int_0^a\left\{\int_{-\frac{h}{2}}^{\frac{h}{2}}\left[-m\beta\delta(\delta-1)t^{\delta-2}z_2+m\omega^2\left(\frac{h}{2}-z_2\right)(a-x)\right]z_2dz_2\right\}dx. \tag{65}$$

The curvature and the coordinate of the neutral axis are obtained from (61) and (62) by the MatLab. Then, integration in (53) is carried-out by the MatLab.

Formula (66) is applied for deriving J_{L3}.

$$J_{L3}=\int\left[u_{0L3}\cos\alpha_{L3}-\left(p_{xcrL3}\frac{\partial u_{L3}}{\partial x_{cr}}+p_{ycrL3}\frac{\partial v_{L3}}{\partial x_{cr}}\right)\right]dL_3, \tag{66}$$

where

$$u_{0L3}=\int\sigma_{L3}d\varepsilon_{L3}, \tag{67}$$

$$\cos\alpha_{L3}=-1, \tag{68}$$

$$p_{xcrL3}=-\sigma_{L3}, \tag{69}$$

$$\frac{\partial u_{L3}}{\partial x_{cr}}=\varepsilon_{L3}, \tag{70}$$

$$p_{ycrL3}=0, \tag{71}$$

$$dL_3=dz_3, \tag{72}$$

$$-\frac{h_1}{2}\le z_3\le\frac{h_1}{2}. \tag{73}$$

Here, h_1 is the thickness of the crack upper arm, z_3 is the vertical centric axis. The curvature and the coordinate of the neutral axis of the cross-section, L_3, of the crack upper arm are determined from Eqs. (74) and (75).

$$N_{L3}=b\int_{-\frac{h_1}{2}}^{\frac{h_1}{2}}\sigma_{L3}dz_3, \tag{74}$$

$$M_{L3}=b\int_{-\frac{h_1}{2}}^{\frac{h_1}{2}}\sigma_{L3}z_3dz, \tag{75}$$

where the axial force and the bending moment are obtained by analyzing the equilibrium of the crack upper arm under the forces of inertia, i.e.

$$N_{L3} = b\int_0^a \left(\int_{-\frac{h_1}{2}}^{\frac{h_1}{2}} -m\beta\delta(\delta-1)t^{\delta-2}dz_3 \right) dx, \tag{76}$$

$$M_{L3} = b\int_0^a \left\{ \int_{-\frac{h_1}{2}}^{\frac{h_1}{2}} \left[-m\beta\delta(\delta-1)t^{\delta-2}z_3 + m\omega^2\left(h_2 + \frac{h_1}{2} - z_3\right)(a-x) \right] z_3 dz_3 \right\} dx. \tag{77}$$

The integral in (66) is solved by the MatLab. Then, J is found by inserting of J_{L1}, J_{L2} and J_{L3} in formula (38).

The integral J solution is confirmed by deriving the strain energy release rate (SERR) for the moving bar in Fig. 1. The SERR, G, is extracted from the complementary strain energy, U^*, cumulated in the bar by using formula (78), i.e.

$$G = \frac{dU^*}{bda}, \tag{78}$$

where

$$U^* = U^*_{D1D2lw} + U^*_{D2D3} + U^*_{D1D2up}. \tag{79}$$

The complementary strain energies in the crack lower arm, the intact portion of the bar and the crack upper arm are determined by formulas (80), (81) and (82), respectively.

$$U^*_{D1D2lw} = \iiint_{(V_{D1D2lw})} u^*_{0D1D2lw} dV, \tag{80}$$

$$U^*_{D2D3} = \iiint_{(V_{D2D\Sigma})} u^*_{0D2D3} dV, \tag{81}$$

$$U^*_{D1D2up} = \iiint_{(V_{D1D2up})} u^*_{0D1D2up} dV, \tag{82}$$

where V_{D1D2lw}, V_{D2D3} and V_{D1D2up} are the volumes of the crack lower arm, the intact portion of the bar and the crack upper arm, respectively. The specific complementary strain energies involved in formulas (80), (81) and (82) are written as given below.

$$u^*_{0D1D2lw} = \sigma_{D1D2lw}\varepsilon_{D1D2lw} - \int \sigma_{D1D2lw} d\varepsilon_{D1D2lw}, \tag{83}$$

$$u^*_{0D2D3} = \sigma_{D2D3}\varepsilon_{D2D3} - \int \sigma_{D2D3} d\varepsilon_{D2D3}, \tag{84}$$

$$u^*_{0D1D2up} = \sigma_{D1D2up}\varepsilon_{D1D2up} - \int \sigma_{D1D2up} d\varepsilon_{D1D2up}. \tag{85}$$

The stresses and strains involved in formulas (83), (84) and (85) are determined by analyzing

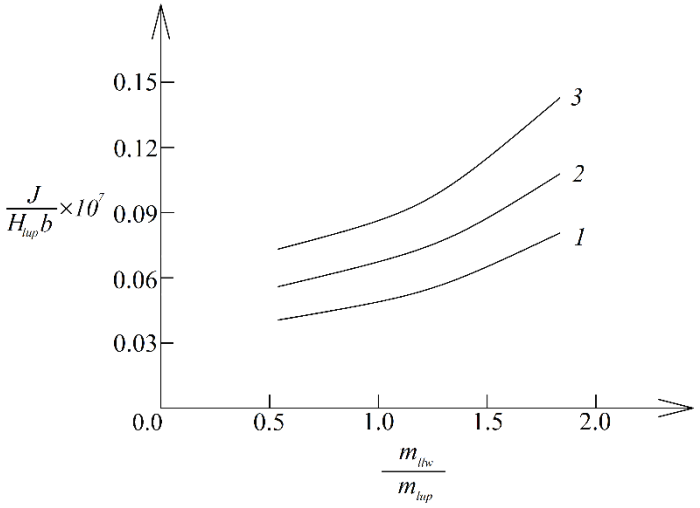

Fig. 3 The integral J-m_{llw}/m_{lup} ratio diagrams (1-at $\beta = 0.0002$ m/s, 2-at $\beta = 0.0004$ m/s and 3-at $\beta = 0.0006$ m/s)

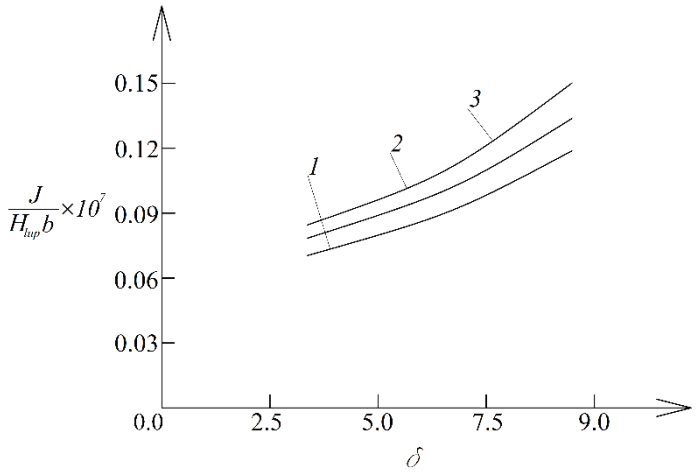

Fig. 4 The integral J-δ diagrams (1-at $m_{rlw}/m_{rup} = 0.5$, 2-at $m_{rlw}/m_{rup} = 1.0$ and 3-at $m_{rlw}/m_{rup} = 2.0$)

the equilibrium of elementary forces in cross-sections of the crack arms and the intact portion of the bar. The SERR derived by (78) matches the integral J. This fact is a verification of the solution of the integral J.

3. Results of the analysis

The results presented in this section of the paper show how the lengthwise fracture behavior of the moving bar is influenced by the parameters of the laws of motion (1) an (2), the continuous material inhomogeneity along the length and thickness of the bar, and the crack length. The change

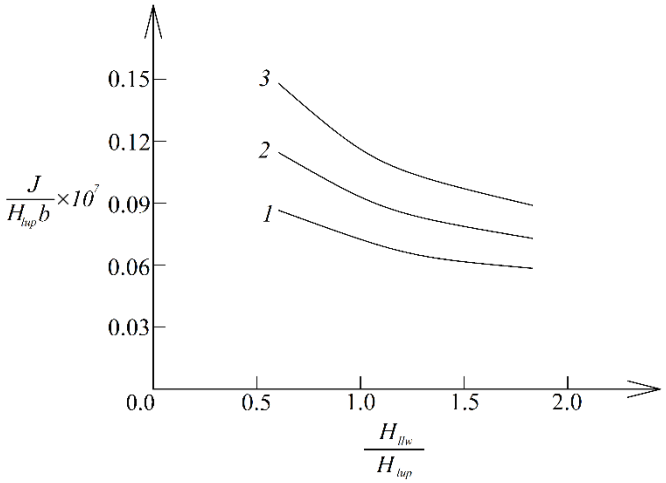

Fig. 5 The integral J-H_{llw}/H_{lup} ratio diagrams (1-at $\lambda = 150$ 1/s, 2-at $\lambda = 300$ 1/s and 3-at $\lambda = 450$ 1/s)

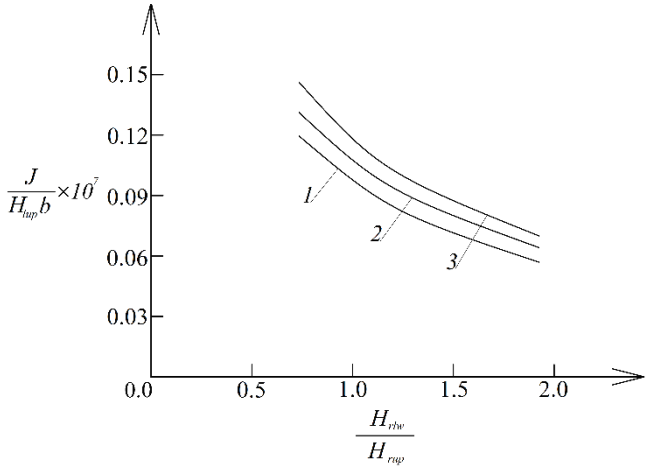

Fig. 6 The integral J-H_{rlw}/H_{rup} ratio diagrams (1-at $\gamma_{llw}/\gamma_{lup} = 0.5$, 2-at $\gamma_{llw}/\gamma_{lup} = 1.0$ and 3-at $\gamma_{llw}/\gamma_{lup} = 2.0$)

of the integral J is presented in form of various diagrams. The following data are used: $b = 0.004$ m, $h = 0.010$ m, $l = 0.400$ m, $h_1 = 0.006$ m, $\eta = 0.4$, $\mu = 0.4$, $\rho = 0.4$, $\psi_H = 0.5$, $\theta_H = 0.5$, $\chi_H = 0.5$, $\psi_\gamma = 0.6$, $\theta_\gamma = 0.6$, $\chi_\gamma = 0.6$, $\psi_T = 0.7$, $\theta_T = 0.7$, $\chi_T = 0.7$, $\psi_\varphi = 0.8$, $\theta_\varphi = 0.8$ and $\chi_\varphi = 0.8$.

Fig. 3 shows the integral J - m_{llw}/m_{lup} ratio diagrams for three values of the parameter, β.

It should be noted that the m_{llw}/m_{lup} ratio reflects the change of the mass per unit area along the left-end of the bar while β is one of the parameters controlling the non-uniform motion of the bar in horizontal direction. In other words, the diagrams depicted in Fig. 3 give an idea for influence of mass distribution and the horizontal motion on the lengthwise fracture behavior of the bar. The integral J in Fig. 3 is normalized by using the formula $J/(H_{lup}b)$. The change of m_{rgh}/m_{lft} ratio presented along the abscissa in Fig. 3 indicates growth of the integral J value. The

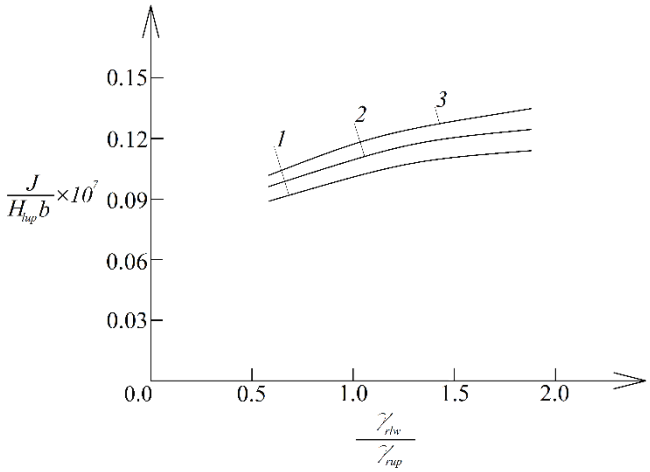

Fig. 7 The integral J-$\gamma_{rlw}/\gamma_{rup}$ ratio diagrams (1-at $T_{rlw}/T_{rup} = 0.5$, 2-at $T_{rlw}/T_{rup} = 1.0$ and 3-at $T_{rlw}/T_{rup} = 2.0$)

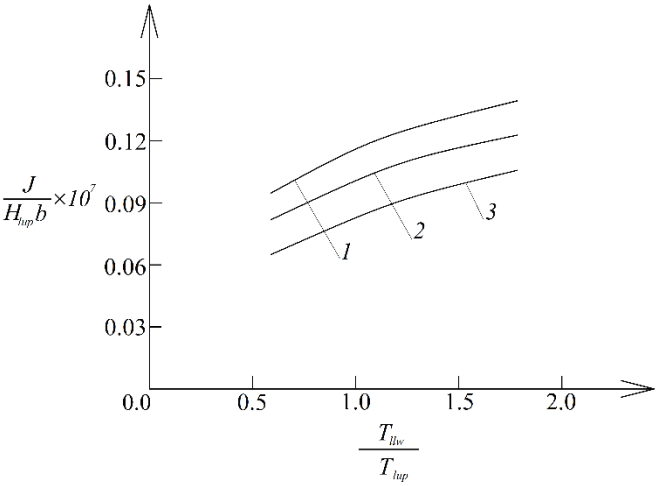

Fig. 8 The integral J-T_{llw}/T_{lup} ratio diagrams (1-at $\varphi_{llw}/\varphi_{lup} = 0.5$, 2-at $\varphi_{llw}/\varphi_{lup} = 1.0$ and 3-at $\varphi_{llw}/\varphi_{lup} = 2.0$)

increase of the value of β also leads to growth of the integral J as shown in Fig. 3.

Fig. 4 presents the integral J-δ diagrams for three m_{rlw}/m_{rup} ratios. The m_{rlw}/m_{rup} ratio characterizes the change of the mass per unit area along the right-hand end of the bar. We observe in Fig. 4 that the response is quite sensitive to the change of m_{rlw}/m_{rup} ratio and the parameter, δ.

The integral J-H_{llw}/H_{lup} ratio diagrams are obtained for three values of the parameter, λ. These diagrams are depicted in Fig. 5. The reason for the growth of the integral J when λ grows which can be observed in Fig. 5 is that the normal acceleration (and the corresponding forces of inertia) increases. Another important observation is the reduction of the integral J value when H_{llw}/H_{lup} ratio grows (Fig. 5). The reason for the reduction is the increase of the bar stiffness.

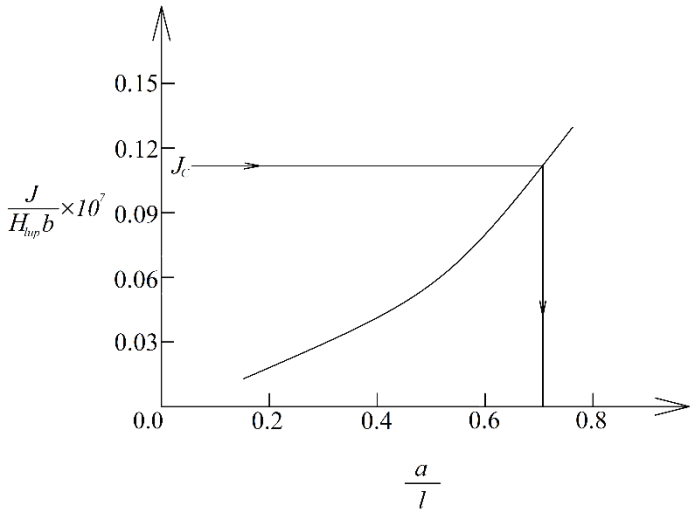

Fig. 9 The integral *J*-a/l ratio diagram

Similar behavior, i.e., reduction of the integral *J*, can be observed also in Fig. 6 where three integral *J* - H_{rlw}/H_{rup} ratio diagrams are depicted. These diagrams are obtained at three $\gamma_{llw}/\gamma_{lup}$ ratios. The growth of $\gamma_{llw}/\gamma_{lup}$ ratio leads to increase of the integral *J* value (Fig. 6).

Fig. 7 presents results for the integral *J* obtained by changing $\gamma_{rlw}/\gamma_{rup}$ and T_{rlw}/T_{rup} ratios. The diagrams in Fig. 7 show growth of the integral *J*.

Analogical behavior, i.e., growth of the integral *J*, is observed also in Fig. 8 where three diagrams illustrating the influence of T_{llw}/T_{lup} and $\varphi_{llw}/\varphi_{lup}$ ratios are depicted.

The analysis developed in this paper can be applied also for determining the critical length of the lengthwise crack in the moving bar in Fig. 1. For this purpose, the integral *J*-a/l ratio diagram is obtained and presented in Fig. 9. The critical length of the crack is the length at which the integral *J* attains the fracture toughness, J_C, as illustrated in Fig. 9. If the crack length is smaller than the critical one, crack growth in the moving bar will not occur.

4. Conclusions

In this paper the problem of lengthwise fracture in a moving bar is addressed. In particular, a bar that movies in horizontal direction and rotates around a horizontal axis is considered. Taking into account the inertia terms in the lengthwise fracture analysis is presented in detail. The bar under consideration is continuously inhomogeneous along the length and thickness. The material nonlinearity also is treated. Because of the inhomogeneity, the mass density, i.e., the mass per unit area, and the parameters of the non-linear constitutive law applied for describing the bar mechanical behavior change continuously along the length and thickness of the bar. The inertia terms also change continuously. The integral *J* is applied in the lengthwise fracture analysis of the bar under the forces of inertia. The solution is confirmed by deriving the SERR. The analysis performed shows that the value of the integral *J* is quite sensitive to the continuous change of mass density along the length and thickness of the bar. For instance, increase of m_{rgh}/m_{lft} and

m_{rlw}/m_{rup} ratios (these ratios characterize the change of mass density along the left and right ends of the bar) induce significant growth of the integral J. The influence of the parameters of the laws for motion of the bar on the integral J is evaluated too. It is found that the value of the integral J grows when the values of the parameters, β, δ and λ, increase. Concerning the effect of continuous change of the parameters of the non-linear constitutive law the analysis reveals the following. The value of integral J reduces when H_{llw}/H_{lup} and H_{rlw}/H_{rup} ratios grow. Increase of the value of integral J is observed when $\gamma_{llw}/\gamma_{lup}$, $\gamma_{rlw}/\gamma_{rup}$, T_{rlw}/T_{rup} and T_{llw}/T_{lup} ratios increase. The analysis is applied also for determining the critical crack length. Concerning the specific laws applied for describing the motion of the bar, the mechanical behavior, the change of the mass density and other material parameters along the length and thickness of the bar, it should be noted that these laws are used here mainly to show the way for application of the approach for analyzing the lengthwise fracture in moving bars developed in the paper. Various laws can be used depending on the problem that is treated.

References

Broek, D. (1986), *Elementary Engineering Fracture Mechanics*, Springer.

Celebi, K. and Tutuncu, N. (2011), "Exact natural frequencies of functionally graded beams via an elasticity approach", *6th International Conference on Composite Structures ICCS 16*, 1-3.

Cetin, A., Uzay, Ç., Tütüncü, N. and Geren, N. (2024), "Predicting the indentation load of FRP facesheet/foam core sandwiches", *Struct.*, **62**, 106266. https://doi.org/10.1016/j.istruc.2024.106266.

Dolgov, M.A. (2024), "Analysis of the stress state in the deformed coating under base stretching with the bending effect account", *Strength Mater.*, **56**, 1127-1135. https://doi.org/10.1007/s11223-025-00723-2.

Dolgov, N.A. (2005), "Determination of stresses in a two-layer coating", *Strength Mater.*, **37**(2), 422-431. https://doi.org/10.1007/s11223-005-0053-7.

Dolgov, N.A. (2016), "Analytical methods to determine the stress state in the substrate-coating system under mechanical loads", *Strength Mater.*, **48**(1), 658-667. https://doi.org/10.1007/s11223-016-9809-5.

Dowling, N.E. (2013), *Mechanical Behaviour of Materials*, Person.

Ellali, M., Amara, K. and Bouazza, M. (2024), "Thermal buckling of porous FGM plate integrated surface-bonded piezoelectric", *Couple. Syst. Mech.*, **13**(4), 171-186. https://doi.org/10.12989/csm.2024.13.2.171.

Gasik, M.M. (2010), "Functionally graded materials: bulk processing techniques", *Int. J. Mater. Prod. Technol.*, **39**(1-2), 20-29. https://doi.org/10.1504/IJMPT.2010.034257.

Hedia, H.S., Aldousari, S.M., Abdellatif, A.K. and Fouda, N.A. (2014), "New design of cemented stem using functionally graded materials (FGM)", *Biomed. Mater. Eng.*, **24**(3), 1575-1588. https://doi.org/10.3233/BME-140962.

Hirai, T. and Chen, L. (1999), "Recent and prospective development of functionally graded materials in Japan", *Mater. Sci. Forum*, **308-311**(4), 509-514. https://doi.org/10.4028/www.scientific.net/MSF.308-311.509.

Hung, P.T., Nguyen-Xuan, H., Phung-Van, P. and Thai, C.H. (2024), "Modified strain gradient analysis of the functionally graded triply periodic minimal surface microplate using isogeometric approach", *Eng. Comput.*, **40**, 2877-2904. https://doi.org/10.1007/s00366-023-01942-4.

Hung, P.T., Phung-Van, P. and Thai, C.H. (2023), "Small scale thermal analysis of piezoelectric-piezomagnetic FG microplates using modified strain gradient theory", *Int. J. Mech. Mater. Des.*, **19**, 739-761. https://doi.org/10.1007/s10999-023-09651-y.

Mahamood, R.M. and Akinlabi, E.T. (2017), *Functionally Graded Materials*, Springer.

Markworth, A.J., Ramesh, K.S. and Parks, Jr. W.P. (1995), "Review: Modeling studies applied to functionally graded materials", *J. Mater. Sci.*, **30**(3), 2183-2193. https://doi.org/10.1007/BF01184560.

Miyamoto, Y., Kaysser, W.A., Rabin, B.H., Kawasaki, A. and Ford, R.G. (1999), *Functionally Graded Materials: Design, Processing and Applications*, Kluwer Academic Publishers, Dordrecht/London/Boston.

Mokhefi, D., Bessaim, A., Houari, M.S.A., Deffane, Z., Houari-Belkadi, H., Ali, B., ... & Merzouki, T. (2024), "A nonlocal strain gradient model for buckling analysis of advanced FG CNT-reinforced composite nanobeams", *Couple. Syst. Mech.*, **13**(5), 375-393. https://doi.org/10.12989/csm.2024.13.5.375.

Nemat-Allal, M.M., Ata, M.H., Bayoumi, M.R. and Khair-Eldeen, W. (2011), "Powder metallurgical fabrication and microstructural investigations of Aluminum/Steel functionally graded material", *Mater. Sci. Appl.*, **2**(5), 1708-1718. https://doi.org/10.4236/msa.2011.212228.

Phung-Van, P., Nguyen, L.B., Hung, P.T., Nguyen-Xuan, H. and Thai, C.H. (2024), "Nonlocal nonlinear analysis of functionally graded piezoelectric porous nanoplates", *Int. J. Mech. Mater. Des.*, **20**, 743-753. https://doi.org/10.1007/s10999-023-09701-5.

Phung-Van, P., Nguyen-Xuan, H. and Thai, C.H. (2023), "Nonlocal strain gradient analysis of FG GPLRC nanoscale plates based on isogeometric approach", *Eng. Comput.*, **39**, 857-866. https://doi.org/10.1007/s00366-022-01689-4.

Rabia, B., Daouadji, T.H. and Abderezak, R. (2023), "Mechanical behavior of RC beams bonded with thin porous FGM plates: Case of fiber concretes based on local materials from the mountains of the Tiaret highlands", *Couple. Syst. Mech.*, **12**(3), 241-260. https://doi.org/10.12989/csm.2023.12.3.241.

Rezaiee-Pajand, M. and Masoodi, A.R. (2022), "Hygro-thermo-elastic nonlinear analysis of functionally graded porous composite thin and moderately thick shallow panels", *Mech. Adv. Mater. Struct.*, **29**(4), 594-612. https://doi.org/10.1080/15376494.2020.1780524.

Rezaiee-Pajand, M. and Masoodi, A.R. (2019), "Stability analysis of frame having FG tapered beam-column", *Int. J. Steel Struct.*, **19**, 446-468. https://doi.org/10.1007/s13296-018-0133-8.

Rezaiee-Pajand, M., Masoodi, A.R. and Mokhtari, M. (2018), "Static analysis of functionally graded non-prismatic sandwich beams", *Adv. Comput. Des.*, **3**, 165-190. https://doi.org/10.12989/acd.2018.3.2.165165.

Rezaiee-Pajand, M., Mokhtari, M. and Masoodi, A.R. (2018), "Stability and free vibration analysis of tapered sandwich columns with functionally graded core and flexible connections", *CEAS Aeronaut. J.*, **9**, 629-648. https://doi.org/10.1007/s13272018-0311-6.

Rizov, V. (2025), "Longitudinal fracture analysis of continuously inhomogeneous beams undergoing general planar motion", *J. Appl. Comput. Mech.*, 1-13. https://doi.org/10.22055/jacm.2025.48102.4977.

Rizov, V.I. (2021), "Viscoelastic inhomogeneous beam under time-dependent strains: A longitudinal crack analysis", *Adv. Comput. Des.*, **6**(2), 153-168. https://doi.org/10.12989/acd.2021.6.2.153153.

Rizov, V.I. (2022), "Effects of periodic loading on longitudinal fracture in viscoelastic functionally graded beam structures", *J. Appl. Comput. Mech.*, **8**(1), 370-378. https://doi.org/10.22055/JACM.2021.37953.3141.

Rizov, V.I. (2024), "The effect of delamination between layers in U-shaped members made of functionally graded multilayered viscoelastic materials", *J. Appl. Comput. Mech.*, **10**, 830-841. https://doi.org/10.22055/jacm.2024.46014.4449.

Rizov, V.I. (2017), "Analysis of longitudinal cracked two-dimensional functionally graded beams exhibiting material non-linearity", *Frattura ed Integrità Strutturale*, **41**, 498-510. https://doi.org/10.3221/IGF-ESIS.41.61.

Rizov, V.I. and Altenbach, H. (2019), "On the analysis of lengthwise fracture of functionally graded round bars", *Struct. Integr. Life*, **19**(2), 102-108.

Tsankov, T. (1996), *Theory of Plasticity*, Science.

Tutuncu, N. (2007), "Stresses in thick-walled FGM cylinders with exponentially-varying properties", *Eng. Struct.*, **29**, 2032-2035. https://doi.org/10.1016/j.engstruct.2006.12.003.

Tutuncu, N. and Ozturk, M. (2001), "Exact solutions for stresses in functionally graded pressure vessels", *Compos. Part B: Eng.*, **32**, 683-686. https://doi.org/10.1016/S1359-8368(01)00041-5.

Tutuncu, N. and Temel, B. (2013), "An efficient unified method for thermoelastic analysis of functionally graded rotating disks of variable thickness", *Mech. Adv. Mater. Struct.*, **20**, 38-46.

https://doi.org/10.1080/15376494.2011.581413.
Yildirim, S. and Tutuncu, N. (2019), "Effect of magneto-thermal loads on the rotational instability of heterogeneous rotors", *AIAA J.*, **57**, 2069-2074. https://doi.org/10.2514/1.J058124.